Chemical Engineering Journal 334 (2018) 2004–2013

Contents lists available at ScienceDirect

Chemical Engineering Journal

journal homepage: www.elsevier.com/locate/cej

Nitrogen-rich hyper-crosslinked polymers for low-pressure CO_2 capture

Kehinde A. Fayemiwo[a], Goran T. Vladisavljević[a,*], Seyed Ali Nabavi[a,b], Brahim Benyahia[a], Dawid P. Hanak[b], Konstantin N. Loponov[a], Vasilije Manović[b,*]

[a] Department of Chemical Engineering, Loughborough University, Loughborough LE11 3TU, United Kingdom
[b] Combustion and CCS Centre, Cranfield University, Cranfield MK43 0AL, United Kingdom

GRAPHICAL ABSTRACT

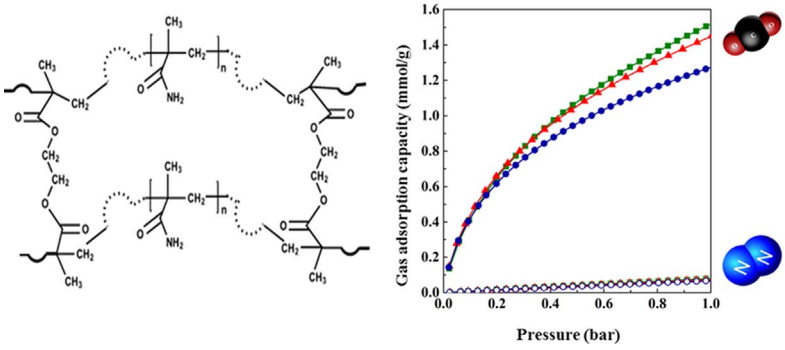

ARTICLE INFO

Keywords:
Amine and amide groups
CO_2 solid adsorbent
Hyper-crosslinked polymeric particles
Methacrylamide
Carbon capture and storage
Post-combustion CO_2 capture

ABSTRACT

A series of poly[methacrylamide-co-(ethylene glycol dimethacrylate)] (poly(MAAM-co-EGDMA)) porous polymeric particles with high CO_2-philicity, referred to as HCP-MAAMs, were synthesised for CO_2 capture. The polymers with a MAAM-to-EGDMA molar ratio from 0.3 to 0.9 were inherently nitrogen-enriched and exhibited a high affinity towards selective CO_2 capture at low pressures. A techno-economic model based on a 580 MW_{el} supercritical coal-fired power plant scenario was developed to evaluate the performance of the synthesised adsorbents. The presence and density of NH_2 moieties within the polymer network were determined using Fourier transform infrared (FTIR) spectroscopy and X-ray photoelectron spectroscopy (XPS). The thermogravimetric analysis (TGA) showed that the polymers were thermally stable up to 515–532 K. The maximum CO_2 adsorption capacity at 273 K was 1.56 mmol/g and the isosteric heat of adsorption was 28–35 kJ/mol. An increase in the density of amide groups within the polymer network resulted in a higher affinity towards CO_2 at low pressure. At a CO_2:N_2 ratio of 15:85, CO_2/N_2 selectivity at 273 K was 52 at 1 bar and reached 104 at ultra-low CO_2 partial pressure. The techno-economic analysis revealed that retrofitting a HCP-MAAM-based CO_2 capture system led to a net energy penalty of 7.7–8.0%$_{HHV}$ points, which was noticeably lower than that reported for MEA or chilled ammonia scrubbing capture systems. The specific heat requirement was superior to the majority of conventional solvents such as MDEA-PZ and K_2CO_3. Importantly, the economic performance of the HCP-MAAM retrofit scenario was found to be competitive to chemical solvent scrubbing scenarios.

* Corresponding authors.
E-mail addresses: g.vladisavljevic@lboro.ac.uk (G.T. Vladisavljević), v.manovic@cranfield.ac.uk (V. Manović).

https://doi.org/10.1016/j.cej.2017.11.106
Received 24 September 2017; Received in revised form 19 November 2017; Accepted 20 November 2017
Available online 21 November 2017
1385-8947/ © 2017 The Authors. Published by Elsevier B.V. This is an open access article under the CC BY license (http://creativecommons.org/licenses/BY/4.0/).

1. Introduction

Carbon capture and storage (CCS) is considered as the most viable pathway to cut CO_2 emissions from the power and industrial sectors and mitigate the severe consequences of global warming and climate change [1–3]. Carbon capture is the initial but most expensive step in CCS. Post-combustion capture (PCC) is the most feasible short-to-medium term capture technology due to its ease of retrofitting to existing power plants and industries without major modifications [4]. Monoethanolamine (MEA) scrubbing is currently recognised as the benchmark PCC technology [4]. However, MEA requires high energy for regeneration, which inevitably leads to high energy penalties for power plants [5]. Also, MEA is corrosive and the presence of its degradation products in PCC emissions has raised concern over their potential impact on human health and the environment [6]. Solid adsorbents, such as zeolites, activated carbons, metal-organic frameworks (MOFs), functionalised silicas, and polymers, are non-corrosive, environmentally friendly materials, associated with lower energy consumption for regeneration and thus, are considered to be promising substitutes for MEA [7–11]. An ideal solid adsorbent for PCC should have: (1) high CO_2 selectivity; (2) acceptable CO_2 adsorption capacity; (3) low heat of adsorption; (4) high hydrochemical stability; (5) high thermal and mechanical stability; (6) stable cyclic adsorption capacity; (7) production scalability; (8) suitable morphology; (9) low price; and (10) minimal corrosivity and toxicity [4,7,12–14].

Chemisorptive adsorbents form strong covalent bonds with CO_2, which are typically associated with high heat of adsorption (> 40 kJ/mol). On the other hand, physical adsorption is affected mainly by van der Waals forces, which are significantly weaker. Therefore, the heat of adsorption for physisorptive adsorbents, such as polymers, is relatively low (20–40 kJ/mol), which greatly reduces the required regeneration energy in PCC [15]. In addition, high CO_2 selectivity at low pressures is a key factor in the selection of CO_2 adsorbents for a temperature swing adsorption (TSA) process. Therefore, a physical adsorbent with a sufficiently high CO_2 selectivity and capture capacity can be a promising alternative to conventional materials for PCC. However, one of the main disadvantages of physisorptive adsorbents is their low CO_2 selectivity. For example, COP-4 (covalent organic polymer), synthesised by Xiang et al. [16] exhibited a high CO_2 adsorption capacity of ~ 2 mmol/g at 298 K and 0.15 bar CO_2 partial pressure, but its selectivity was below 10. Adsorbents with low selectivity cannot provide an acceptable separation efficiency, and require additional CO_2 purification that results in increased capital and operational costs [17]. Amongst gas species in a typical flue gas, CO_2 has the highest quadruple moment and polarisability [18]. Therefore, an effective strategy to synthesise physical adsorbents with high CO_2 selectivity is to formulate their chemistry with protic electronegative functionalities, usually by introducing polar nitrogen-containing groups, such as amine and amide [15,19,20].

The morphology of the synthesised adsorbents and their production scalability are other important parameters that have often been neglected [21]. The majority of adsorbents are produced as fine powders, which are not practical for commercial CO_2 capture systems, such as fixed and fluidised bed reactors. Fine particles often need to be pelletised, which may change their performance and impose extra costs [14,20,22,23]. Zhao et al. [24] fabricated amide-based molecularly-imprinted polymers (CO_2-MIPs) using oxalic acid as a template, via bulk polymerisation, and achieved high CO_2 selectivity combined with a low heat of adsorption. However, the heat released due to the exothermic nature of the polymerisation reaction and poor heat transfer can destabilise the monomer-template complex and reduce the number of CO_2-selective sites. Nabavi et al. [25] fabricated MIPs using suspension polymerisation to facilitate heat transfer during the polymerisation process and improve the particle morphology and yield. However, due to difficulties in removing the template from the polymer to make the cavities available to CO_2 [26], the process can be challenging for large-scale production.

In this study, a series of nitrogen-rich, hyper-crosslinked poly[methacrylamide-co-(ethylene glycol dimethacrylate)] polymers (HCP-MAAMs) suitable for CO_2 capture were synthesised through bulk co-polymerisation. The polymers were inherently amine-functionalised and showed a high CO_2/N_2 selectivity at low CO_2 partial pressures. A detailed physicochemical characterisation of the polymer particles was performed and their performance under typical PCC conditions was investigated. In addition, a techno-economic model was developed to assess the feasibility of the synthesised material as a CO_2 capture sorbent in a 580 MW_{el} supercritical coal-fired power plant.

2. Material and methods

2.1. Materials

Acetonitrile (ACN) was purchased from Fisher Scientific, UK. Ethylene glycol dimethacrylate (EGDMA), methacrylamide (MAAM), and azobisisobutyronitrile (AIBN) were supplied by Sigma Aldrich, UK. All the reagents were of analytical grade. A Millipore Milli-Q Plus 185 water purification system was used to provide pure water. All the gases were supplied by BOC, UK, with a purity higher than 99.999%.

2.2. Polymer synthesis

For each sample, 12–36 mmol of MAAM (monomer), 40 mmol of EGDMA (crosslinker), and 0.6 mmol of AIBN (initiator) were dissolved in 30 mL of ACN (porogenic solvent), Table 1. The reaction mixture was degassed by sonication for 10 min, purged with N_2 for another 10 min to remove the dissolved oxygen, and then sealed and polymerised in a water bath at 333 K for 24 h (Fig. 1).

The synthesised monolithic polymer was manually crushed, ground, and sieved to obtain particles with sizes in the range of 90–212 μm. The particles were then washed several times with water, filtered using a Büchner funnel, and dried overnight in a vacuum oven at 353 K. The scanning electron microscope (SEM) micrographs of the fabricated particles are presented in Fig. 2.

2.3. Characterisation methods

2.3.1. Pore structure analysis

The surface properties of the samples were derived from nitrogen adsorption isotherms using a Micromeritics ASAP 2020 Accelerated Surface Area and Porosimetry system at 77 K. Prior to each test, the sample was degassed under vacuum at 353 K overnight. The specific surface area of the samples was estimated from the Brunauer–Emmett–Teller (BET) isotherm equation at the relative pressures, P/P_0 of 0.06–0.30. The total pore volume was calculated at P/P_0 of 0.99. The pore size distribution of the samples was determined from nitrogen desorption isotherms using the Barrett-Joyner-Halenda (BJH) method.

2.3.2. Density measurement

The density of the particles was measured using a helium

Table 1
The specific surface area, S_{BET}, the total pore volume, V_p of the polymer samples prepared using different amounts of MAAM.[a]

Sample	MAAM (mmol)	EGDMA (mmol)	AIBN (mmol)	S_{BET} (m^2/g)	V_p (cm^3/g)
HCP-MAAM-1	12	40	0.6	298	0.47
HCP-MAAM-2	24	40	0.6	142	0.87
HCP-MAAM-3	36	40	0.6	83	0.24

[a] The amount of ACN in the reaction mixture was 30 mL, the polymerisation was carried out at 333 K for 24 h.

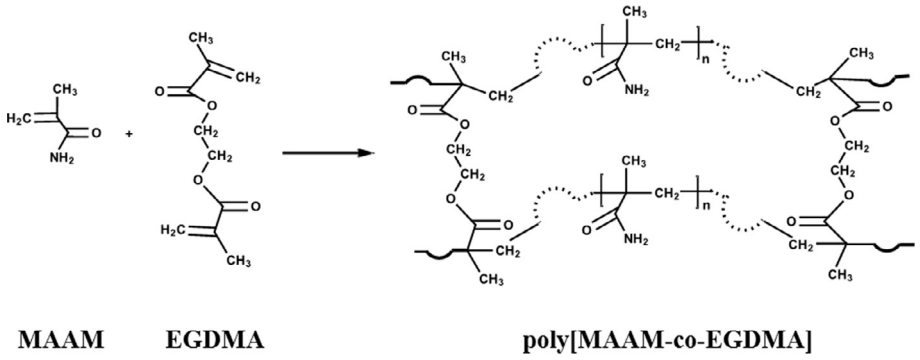

Fig. 1. The synthesis of poly[methacrylamide-co-(ethylene glycol dimethacrylate)], Poly(MAAM-co-EGDMA).

pycnometer (Micromeritics, US). Prior to each test, the particles were dried overnight in a vacuum oven at 353 K. For each sample, five repeated measurements were made and the average value was reported.

2.3.3. Thermal analysis

The thermal stability of the samples was measured using a thermogravimetric analyser (TGA) (Q5000 IR, TA Instruments, US). In each test, up to 15 mg of sample was heated from 323 K to 873 K with a heating rate of 10 K/min under a nitrogen flow rate of 20 mL/min.

2.3.4. X-ray photoelectron spectroscopy (XPS)

XPS experiments were carried out on a K-alpha Thermo Scientific spectrometer using an Al Kα monochromatic X-ray source ($h\nu$ = 1486.4 eV, 36 W power, 400 µm spot size) for radiation and low-energy electron/ion flooding for charge compensation. Survey scan spectra for elemental analysis were acquired using a pass energy of 200 eV, a step size of 1 eV, a dwell time of 10 ms and 15 scans. A pass energy of 50 eV and a step size of 0.1 eV, with a dwell time of 50 ms and 10 scans, was used to obtain high-resolution scans of the N 1s, C 1s, and O 1s peaks. In order to evaluate the XPS data, AVANTAGE software was used, and the background was subtracted using the Shirley methods. The mixed Gaussian-Lorentzian peak shape with 30% Lorentzian character was used to fit the peaks [27].

2.3.5. Fourier transform infrared (FTIR) spectroscopy

FTIR spectra were measured over the range of 500–4000 cm^{-1} using a Thermo Scientific Nicolet iS50 ATR spectrometer with a monolithic diamond crystal. For each test, 2–3 mg of sample was placed on the Universal diamond ATR top-plate and the spectrum was acquired.

2.3.6. SEM

The morphology of the samples was investigated using a benchtop SEM, TM3030 (Hitachi), operating at an accelerating voltage of 15 keV. Prior to scanning, the samples were coated with gold/palladium (80/20) alloy to prevent the accumulation of electrostatic charges on the particles. The sputter coating speed was 0.85 nm/s, at 2 kV applied voltage and 25 mA plasma current.

2.3.7. Adsorption isotherms of CO_2 and N_2

The adsorption isotherms of CO_2 and N_2 in the pressure range of up to 1 bar and at temperatures of 273 K and 298 K were obtained using a Micromeritics ASAP 2020 static volumetric apparatus equipped with a Micromeritics ISO Controller. Prior to each test, the particles were degassed under vacuum at 353 K overnight.

2.3.8. Dynamic CO_2 capture using polymer-based material

The recyclability of the samples was assessed based on the dynamic CO_2 adsorption-desorption measurement using a fixed-bed column packed with 2 g of the adsorbent [13,14]. CO_2 adsorption was performed by passing a 15% CO_2/85% N_2 (v/v) simulated gas mixture through the bed at 298 K and 130 mL/min, and continued until adsorption equilibrium was reached. The residence time of HCP-MAAM-2 sample (80 s) was calculated from the adsorption breakthrough curve shown in Fig. S1 in Supplementary Information. The desorption was carried out by purging the sample with nitrogen for 90 min at 393 K and 130 mL/min. To confirm that CO_2 can be desorbed below 393 K, a CO_2-saturated sample was exposed to 60 mL/h N_2 flow over the temperature range of 298–361 K. The adsorbed CO_2 was completely released over the temperature range of 298–327 K and no CO_2 was detected in the effluent stream above 327 K (Fig. S2 in Supplementary Information). Moreover, TGA data collected over the temperature range of 303–403 K and under a nitrogen flow rate of 20 mL/min confirmed that impurities and guest molecules were completely removed at 333 K or above (Fig. S3 in Supplementary Information). The adsorption-desorption cycle was repeated five times.

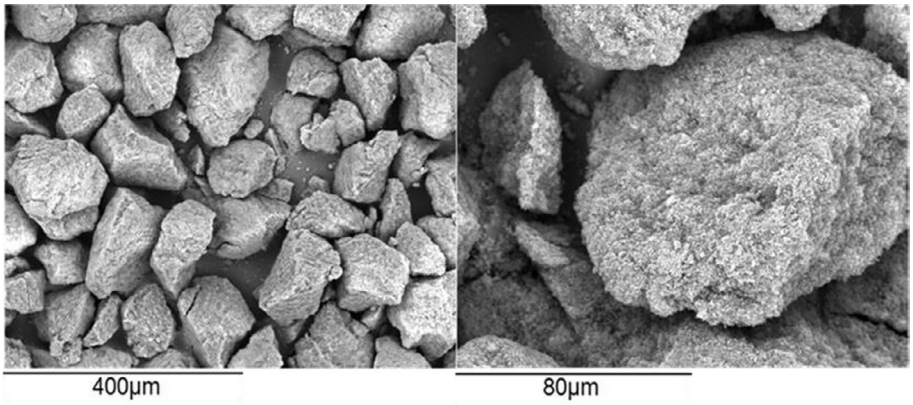

Fig. 2. The SEM images of the fabricated sorbent polymer particles.

Table 2
Supercritical coal-fired power plant key performance parameters.

Parameter	Value
Gross power output (MW_{el})	580.4
Net power output (MW_{el})	552.7
Net thermal efficiency ($\%_{HHV}$)	38.5
Flue gas stream (kg/s)	617.2
CO_2 content in flue gas ($\%_{vol}$)	15.2
Coal consumption rate (kg/s)	53.8
Air consumption rate (kg/s)	526.5
Live steam generation rate (kg/s)	462.3
Excess air ratio ($\%_{vol}$)	20.0
Live steam pressure (bar)	242.3
Reheated steam pressure (bar)	45.2
Intermediate-/low-pressure crossover pipe pressure (bar)	9.3
Condenser pressure (bar)	0.069
Live and reheated steam temperature (K)	866.3
Mechanical efficiency of the rotational machinery (%)	99.0

2.4. Techno-economic model description

2.4.1. Supercritical coal-fired power plant

The 580 MW_{el} supercritical coal-fired power plant was considered as a reference system in this study. The plant model consisting of supercritical boiler, flue gas treatment train, and steam cycle sub-models, has previously been developed [28,29] and validated with the data available in a NETL report [30]. The key performance parameters of the model are provided in Table 2.

Sorbent regeneration takes place at 353 K with the heat required being provided by direct contact of the sorbent with steam extracted from the steam cycle (Fig. S4 in Supplementary Information). Such configuration was claimed to be the most efficient option for providing heat for solvent regeneration in mature chemical solvent scrubbing systems [16]. Moreover, the retrofit scenario is based on a dual intermediate-/low-pressure crossover pressure system with heat integration [29] that ensures that the steam is delivered to the CO_2 capture system at the temperature and pressure required for HCP-MAAM sorbent regeneration.

Importantly, steam extraction from the steam cycle causes off-design operation of the low-pressure turbine [29,31]. Therefore, the power output is not only affected by the reduced low-pressure turbine throughput, but also by the loss in the inlet pressure and the isentropic pressure of this turbine cylinder. These are accounted for using the off-design framework developed by Hanak et al. [31].

2.4.2. CO_2 capture system using polymer-based material

A process flow diagram of the modelled capture system is shown in Fig. 3 and the properties of the sorbent particles used in the design are listed in Table S1. It was assumed that the adsorption and desorption of CO_2 took place in two interconnected fluidised beds, each operating with a pressure drop of 200 mbar. To ensure favourable operating conditions in the adsorber, which is modelled as a conversion reactor, flue gas from the coal-fired power plant is cooled in the direct contact cooler to 298 K. The flash calculations are performed using the Rachford-Rice equation [32] and the process streams are characterised using the Peng Robinson equation of state.

The amount of CO_2 adsorbed at the end of each adsorption step was assumed to be 70% of the CO_2 adsorption capacity, which is a common assumption for CO_2 capture in a fluidised bed using solid adsorbents [34]. The amount of sorbent in the adsorber was estimated to ensure a CO_2 capture level of 90%. The CO_2-rich sorbent is heated using air preheated by the lean sorbent leaving the desorber, to maximise heat recovery in the system. The preheated CO_2-rich sorbent is further heated to 353 K in the desorber to completely desorb the gases and reclaim the concentrated CO_2 stream. The heat required for sorbent regeneration is provided by direct contact of the CO_2-rich sorbent and steam extracted from the steam cycle. CO_2 is then separated from water vapour by cooling in the water knock-out tower, which is modelled as a direct contact cooler, and sent to the CO_2 compression unit. Part of the condensed water is returned to the steam cycle to balance the amount of steam extracted from the intermediate-/low-pressure crossover pipe. The CO_2 compression unit comprises nine intercooled compression stages, each of which was modelled as a polytropic compression stage with a stage efficiency of 78–80% [35,36], and the pressure ratio and polytropic head not exceeding 3 and 3050 m, respectively [37]. It was assumed that the CO_2 delivery pressure of 110 bar was achieved by a CO_2 pump with an isentropic efficiency of 80% [38].

2.4.3. Techno-economic performance evaluation

Having linked the coal-fired power plant and the CO_2 capture system, the thermodynamic performance was evaluated using the system's net power output (W_{net}) and net thermal efficiency (η_{th}), which is defined in Eq. (1) as the ratio of the net power output and the heat input from fuel combustion (Q_{fuel}). In addition, the environmental performance of the HCP-MAAM retrofit scenario is represented in Eq. (2) as the specific CO_2 emissions (e_{CO_2}), defined as the ratio of CO_2 emission rate (m_{CO_2}) and the net power output.

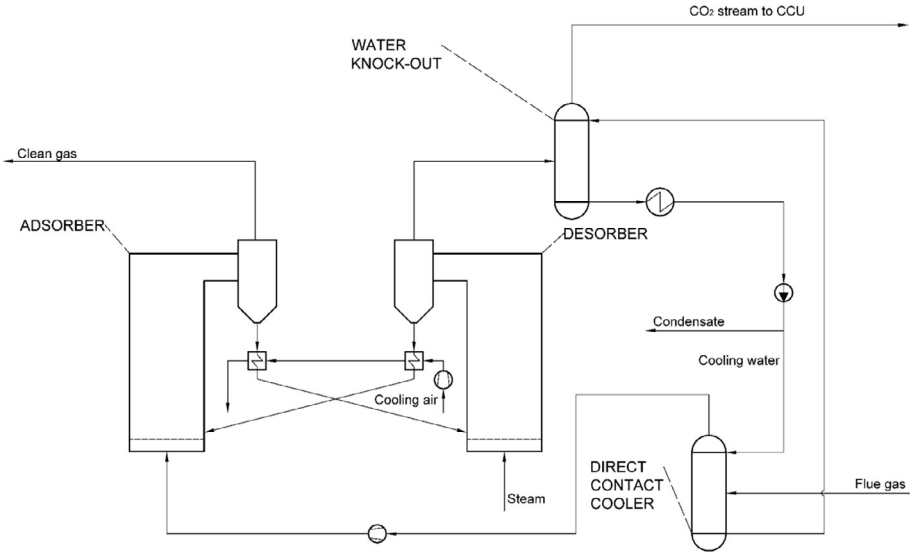

Fig. 3. Process flow diagram of the CO_2 capture system using polymer-based material.

$$\eta_{th} = \frac{W_{net}}{Q_{fuel}} \quad (1)$$

$$e_{CO_2} = \frac{m_{CO_2}}{W_{net}} \quad (2)$$

The economic performance of the proposed system was compared with the reference coal-fired power plant without CO_2 capture using the levelised cost of electricity (*LCOE*) and the cost of CO_2 avoided (*AC*), which are calculated from Eq. (3) and Eq. (4) [39–41], respectively.

$$LCOE = \frac{TCR \times FCF + FOM}{W_{net} \times CF \times 8760} + VOM + \frac{SFC}{\eta_{th}} \quad (3)$$

$$AC = \frac{LCOE_{capture} - LCOE_{ref}}{e_{CO_2,ref} - e_{CO_2,capture}} \quad (4)$$

These parameters correlate thermodynamic performance indicators, such as net power output, net thermal efficiency (η_{th}), capacity factor (*CF*) and specific emissions (e_{CO2}), with economic performance indicators, such as total capital requirement (*TCR*), variable (*VOM*) and fixed (*FOM*) operating and maintenance costs, specific fuel cost (*SFC*), and the fixed charge factor (*FCF*) that considers the system's lifetime and project interest rate.

The capital costs of the coal-fired power plant and the CO_2 capture system (direct contact cooler, water knock-out, pumps and fans, adsorber, desorber, heat exchangers and CO_2 compression unit) were estimated using the exponential method function [42] with economic data gathered from NETL [43] and Woods [44]. In addition, FOM and VOM were calculated as fractions of the total capital cost, while the operating costs associated with fuel consumption, and CO_2 storage, transport and emission were determined based on process simulation outputs using economic data from Table 3.

The physical properties of HCP-MAAM sorbent used in the techno-economic assessment are shown in Table S1. Furthermore, the effect of uncertainty in the sorbent cost on the economic performance was assessed by varying the sorbent cost between 1 and 10,000 £/kg.

3. Results and discussion

3.1. Polymer characterisation

The nitrogen adsorption-desorption isotherms at 77 K, and the pore size distribution curves of the samples are given in Fig. 4. All the samples exhibited Type II isotherms according to the IUPAC classification [45], which is the normal form of isotherm obtained with macroporous or non-porous adsorbents [46]. For all samples, the completion of monolayer coverage occurred at P/P_0 of 0.1 or below and was followed by multilayer adsorption at higher P/P_0 values. The pore sizes ranged between 2 nm and 40 nm, with a distinct peak at ~3.7 nm. An increase in the monomer-to-crosslinker molar ratio in the reaction mixture from 0.3 to 0.9 caused a significant reduction in S_{BET} from 298 to 83 m^2/g, Table 1, that can be attributed to a decrease in the degree of crosslinking of the polymers [24]. However, no correlation between the total pore volume, V_p, and the MAAM content in the reaction mixture was observed, as an increase in MAAM content initially led to an increase in V_p from 0.47 to 0.87 cm^3/g, followed by a reduction to 0.24 cm^3/g.

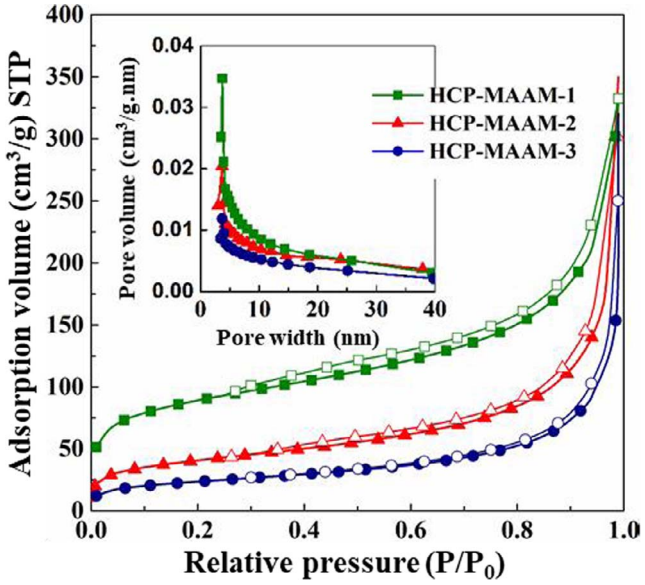

Fig. 4. Nitrogen adsorption-desorption isotherms of the samples at 77 K. The filled and empty symbols represent adsorption and desorption isotherms, respectively. All samples follow Type II isotherms. The inset graph shows the pore size distribution curves of the samples.

Table 3
Key economic model assumptions.

Parameter	Value
Variable cost as a fraction of total capital cost (%) [33,39]	2.0
Fixed cost as a fraction of total capital cost (%) [33,39]	1.0
CO_2 transport and storage cost (£/tCO_2) [40]	7.0
Coal price (£/GJ) [39,41]	1.5
Sorbent cost (£/kg)	8.0
Expected lifetime (years) [33,39]	25
Project interest rate (%) [33,39]	8.78
Capacity factor (%) [33,39]	80
Tax, freight, insurance cost (% of free-on-board supplier cost) [44]	20
Offsite, indirect costs for home office and field expenses (% of labour and material cost including free-on-board supplier cost, freight, delivery, duties and instruments) [44]	30
Contractors fees (% of bare module cost) [44]	4
Project contingency (% of bare module cost) [44]	15
Design contingency (% of bare module cost) [44]	20

Fig. 5a presents the IR spectra of the samples. The peaks at 3440 cm^{-1}, 1633 cm^{-1}, and 910–665 cm^{-1} are associated with N–H stretching, N–H bending, and N–H wagging vibrations, respectively, which confirmed the presence of NH moieties within the polymer network in all samples [14,25]. There was a distinct increase in the intensity of peaks for N–H bending vibration by increasing the MAAM content, which implies the higher density of amide groups within the polymer matrix. This finding was further confirmed and quantified by XPS measurements, Fig. 5b, in which an increase in MAAM to EGDMA molar ratio in the reaction mixture from 0.3 to 0.9 resulted in 2.6 times larger nitrogen content within the polymer matrix.

TGA curves of the samples are shown in Fig. 6. The corresponding onset temperatures of thermal degradation of HCP-MAAM-1, HCP-MAAM-2, and HCP-MAAM-3 were 515 K, 531 K and 532 K, respectively. There was a slight increase in degradation temperature at the higher MAAM-to-EGDMA molar ratio in the reaction mixture, which may be attributed to a lower proportion of thermally unstable ester bonds of EGDMA units in the polymer network. The same trend with noticeably higher thermal stability of the polymer at higher density of amide groups in the polymer network was reported by Nabavi et al. [25] for molecularly-imprinted poly[acrylamide-co-(ethyleneglycol dimethacrylate)] adsorbents. The average true density of the particles measured using a multivolume helium pycnometer was 1.28 g/cm^3.

3.2. CO_2 adsorption assessment

The CO_2/N_2 adsorption isotherms at 273 K and 298 K are presented in Fig. 7a and b. At 273 K, the CO_2 adsorption capacity was found to be 1.56 mmol/g for HCP-MAAM-1, 1.45 mmol/g for HCP-MAAM-2, and 1.28 mmol/g for HCP-MAAM-3 sample. The reduction in the adsorption capacity with an increase in the MAAM content may be attributed to the

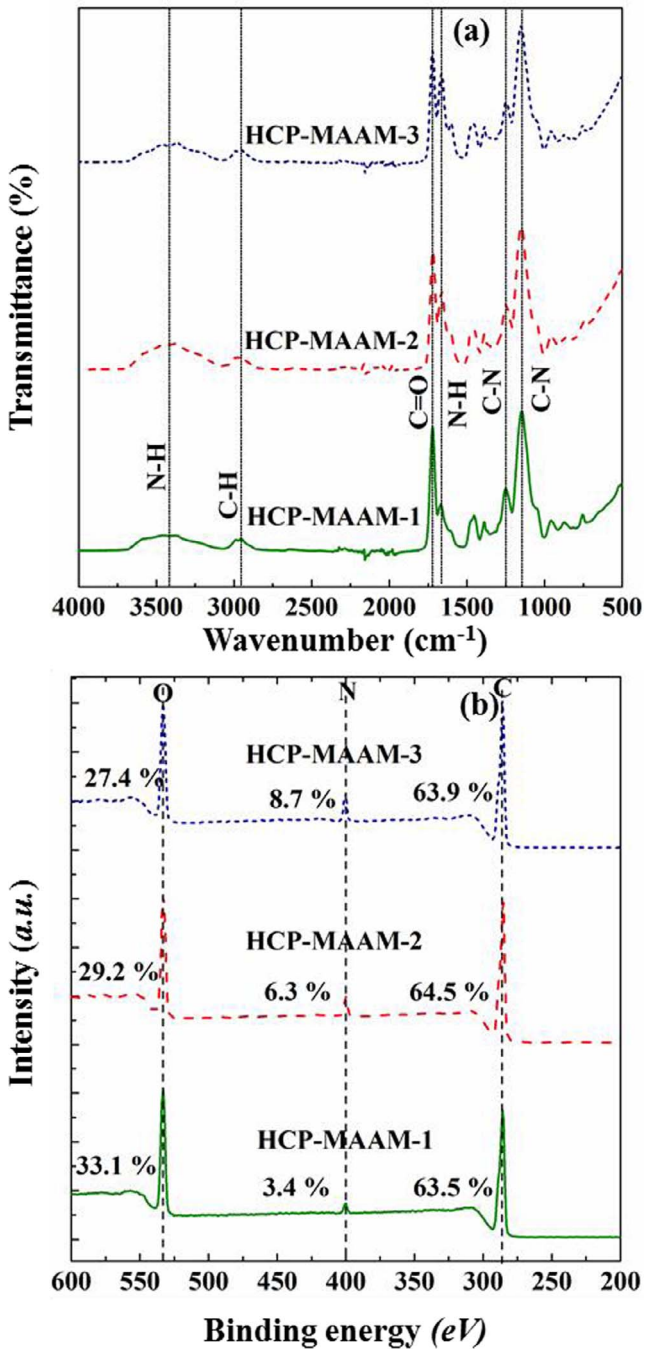

Fig. 5. The surface chemical analysis of the samples: (a) FTIR spectra; (b) XPS spectra including the mass percent of carbon, oxygen, and nitrogen in the polymers.

lower specific surface area of the particles when the EGDMA-to-MAAM molar ratio in the polymer network decreases. Correspondingly, a smaller number of active NH and C═O sites were not exposed on the surface of the particles but incorporated in the interior of the polymer matrix, which in turn, may promote steric hindrance and reduce the diffusion of CO_2 molecules to the active sites [24]. At 298 K, the adsorption capacity of the samples was reduced to 0.92 mmol/g for HCP-MAAM-1, 0.85 mmol/g for HCP-MAAM-2, and 0.79 mmol/g for HCP-MAAM-3. The reduction in CO_2 adsorption capacity at higher temperature is associated with the weaker electrostatic interaction of CO_2 molecules with polar moieties within the polymer matrix.

Fig. 7c and d show the CO_2/N_2 selectivity, S, or separation factor of the samples at 273 K and 298 K as a function of partial pressure of CO_2. The selectivity was calculated using experimental data from the CO_2/N_2 isotherms (Fig. 7a and b), based on the Ideal Adsorbed Solution Theory (IAST) [47,48]:

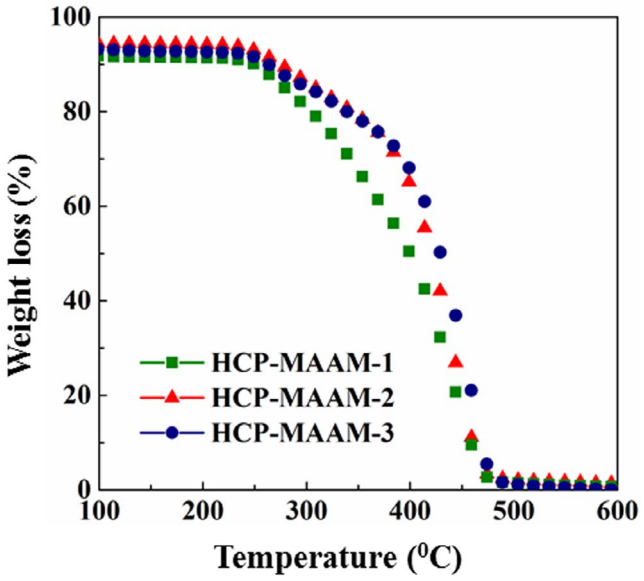

Fig. 6. The TGA curves of the samples over the temperature range of 373–873 K at a heating rate of 10 K/min under nitrogen flow.

$$S = \frac{q_{CO_2}/P_{CO_2}}{q_{N_2}/P_{N_2}} \quad (5)$$

where q and P are the equilibrium adsorption capacity and the partial pressure of the gas species, respectively. The purity of the gas stream after regeneration can be estimated from Eq. (6) [47]:

$$\text{Purity } (\%) = \frac{q_{CO_2}}{q_{N_2} + q_{CO_2}} \times 100 \quad (6)$$

At low CO_2 partial pressure, S was a function of MAAM content and an increase in the MAAM-to-EGDMA ratio resulted in a higher S, Fig. 7c and d. In CO_2-amide interactions, the CO_2 molecule behaves as both Lewis acid (LA) in a LA(CO_2)–LB(C═O) interaction, and Lewis base (LB) in a dipole-dipole interaction with the acidic N–H proton [25,49]. Thus, an increase in the density of polar N–H and C═O moieties within the polymer network increases the affinity of the adsorbent towards CO_2 molecules. At 273 and 0.02–0.15 bar CO_2 partial pressure, the highest S of 104-52 was obtained for HCP-MAAM-3, followed by 99-50 for HCP-MAAM-2, and 86-45 for HCP-MAAM-1. The selectivity of the polymers above a CO_2 partial pressure of ~0.5 bar was very similar for all samples, because at higher pressures, more CO_2 molecules compete for the same number of amide groups and a higher fraction of CO_2 molecules was adsorbed to non-selective sites on the polymer surface. At low CO_2 partial pressure, the interaction between the CO_2 molecules and highly selective CO_2-philic amide groups is a dominant mechanism of the CO_2 adsorption [50]. At 298 K, the selectivity was 72-45 for HCP-MAAM-3, 63-38 for HCP-MAAM-2, and 48-38 for HCP-MAAM-1. The lower selectivity of all the samples at higher temperature can be attributed to the weaker electrostatic interactions between the CO_2 molecules and amide groups in the polymer network. The purity of the gas stream after regeneration of HCP-MAAM-1, HCP-MAAM-2, and HCP-MAAM-3 can be estimated as 90%, 91%, and 91% at 273 K and 88%, 88%, and 90% at 298 K, respectively, based on the typical CO_2 partial pressure in flue gases of coal-fired power plants of 0.15 bar [4]. Therefore, HCP-MAAM-3 can provide the required gas stream purity for storage without any further purification [51], while HCP-MAAM-2 and HCP-MAAM-1 would require an additional CO_2 purification process.

In comparison with existing CO_2 adsorbents, such as COP-4 [16], the HCP-MAAMs mainly benefit from high selectivity which is essential

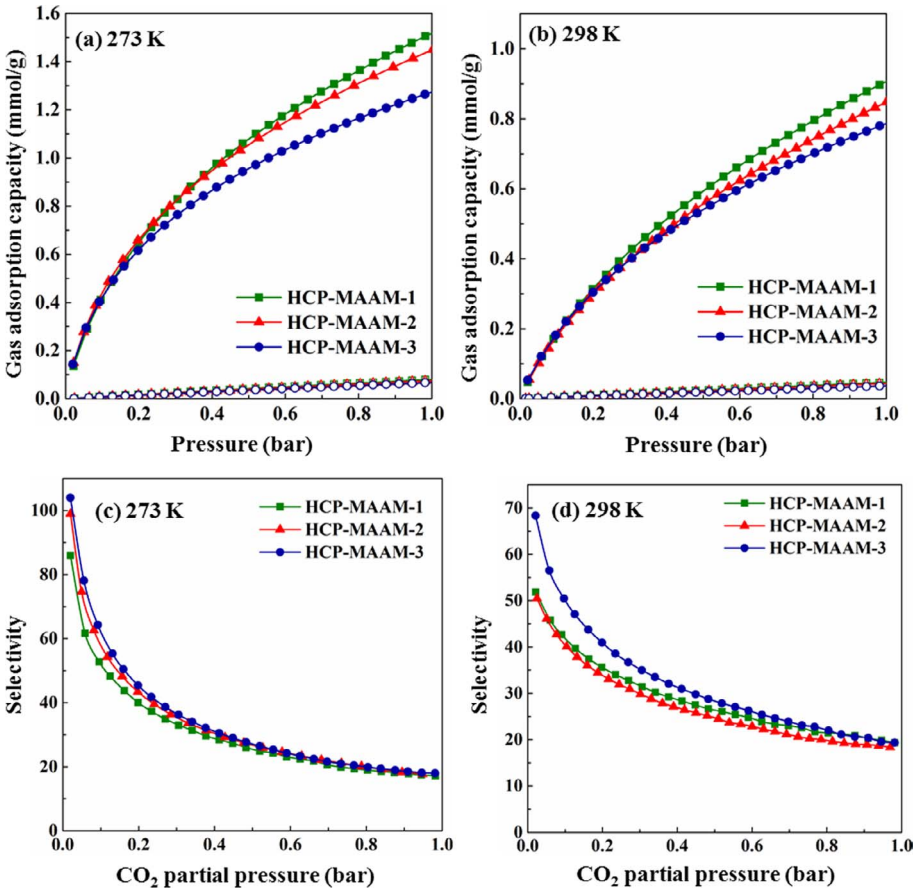

Fig. 7. (a) CO_2 and N_2 adsorption isotherms of the samples at 273 K; (b) CO_2 and N_2 adsorption isotherms of the samples at 298 K. The filled and empty symbols indicate CO_2 and N_2 adsorption isotherms, respectively; (c) CO_2/N_2 selectivity of the samples at 273 K; (d) CO_2/N_2 selectivity of the samples at 298 K.

for industrial PCC applications. At the identical conditions, the adsorption capacity of HCP-MAAMs is better than that of polystyrene microporous organic polymers (MOPs) [52], MOF-aminated graphite oxide (MOF-5/AGO) [53], amide-based MIPs [25] and amidoxime porous polymers [54], and comparable with that of azo-covalent organic polymers (azo-COPs) [15], hyper-crosslinked triazine-based microporous polymers [55], functionalised conjugated microporous polymers (CMP-1-NH_2, CMP-1-COOH) [56], amide-based porous coordination polymers (PCPs) [57], MOF-177 [58], and porous covalent organic frameworks (COF-102) [59]. However, the CO_2 adsorption capacity of HCP-MAAMs was lower than that of polyamine-tethered porous polymeric networks [60], thermoresponsive MOFs [61], sulfonic acid and lithium sulfonate grafted microporous organic polymers (PPN-6-SO_3H, and PPN-6-SO_3Li) [62], potassium intercalated activated carbon [23], Zeolite 13 X [63], Mg-MOF-74 [58], and polyethylenimine functionised porous aromatic frameworks (PAF-5) [64].

Although the selectivity of HCP-MAAMs was high, the CO_2 adsorption capacity at low CO_2 partial pressures (up to 0.15 bar) was relatively low, and needs to be further enhanced, for example, by employing amine-based cross-linkers such as N,N-methylenebis(acrylamide). Moreover, the effect of typical flue gas impurities such as O_2, SO_2 and NO_x on CO_2 adsorption should be evaluated in future studies.

Fig. 8 shows the isosteric heat (enthalpy) of adsorption, Q_{st}, of the samples calculated from the Clausius-Clapeyron equation [65]. For all samples, Q_{st} was in the range between 28 and 35 kJ/mol in the loading range between 0.15 and 0.8 mmol/g. As a comparison, the enthalpy of adsorption of CO_2 with 30 wt% MEA is 80–100 kJ/mol at 313 K in the loading range from 0.04 to 0.4 mole of CO_2 per mole of amine [66], which is 2.5–3 times higher than in this work. The smallest Q_{st} value was obtained for HCP-MAAM-1, which can be attributed to the lowest affinity of this polymer towards CO_2, due to the minimum density of amide groups in the polymer network.

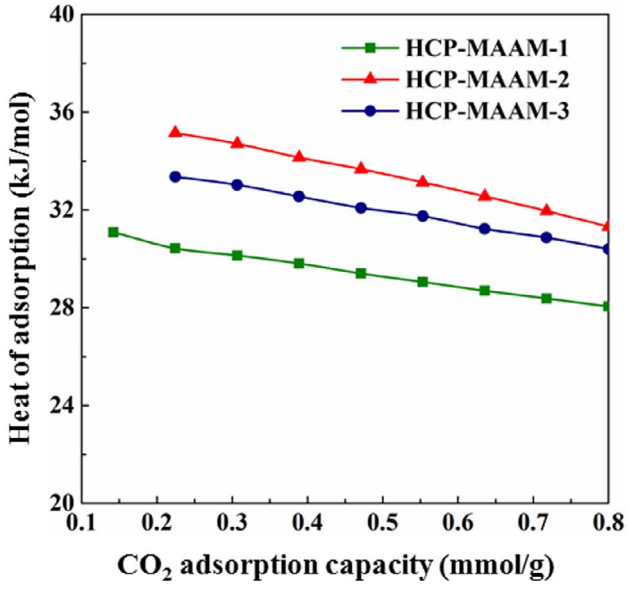

Fig. 8. The isosteric heat of adsorption of the samples.

The cyclic stability of CO_2 adsorption capacity of HCP-MAAM-2 is shown in Fig. 9. In each cycle, CO_2 was adsorbed from a simulated flue gas with a CO_2:N_2 ratio of 15:85 at 1 bar and 298 K, followed by the desorption step under pure N_2 flow at 393 K. Over the five repetitive cycles only a 1.9% reduction in adsorption capacity was observed, which implies a high cyclic CO_2 adsorption stability of the material.

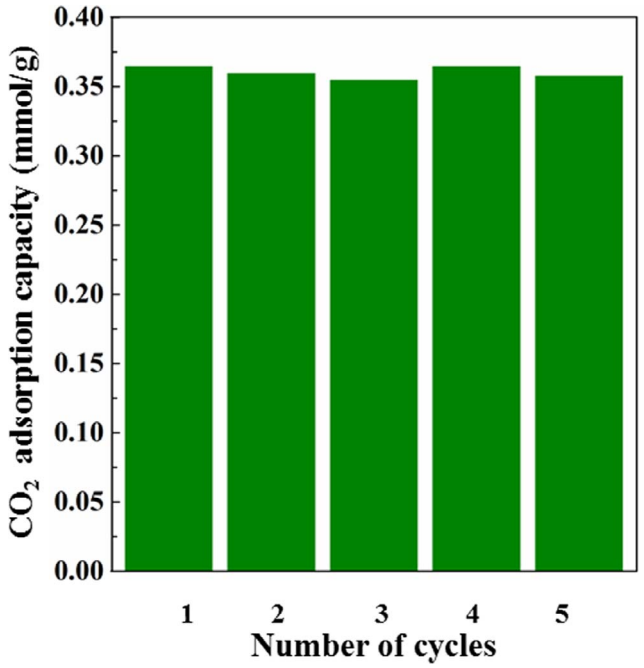

Fig. 9. The dynamic CO_2 adsorption capacity of HCP-MAAM-2 during five repeated cycles at 298 K and 0.15 bar CO_2 partial pressure. The desorption process was performed under N_2 flow at 393 K and 130 mL/h.

3.3. Techno-economic assessment of the material

Retrofitting the CO_2 capture system using HCP-MAAM sorbent to the 580 MW_{el} coal-fired power plant was found to impose a net efficiency penalty of 7.7–8.0%$_{HHV}$ points (Table 4). In addition, the specific coal consumption was found to increase by 25.1–26.0%. The performance of the HCP-MAAM retrofit scenario compares favourably with CO_2 capture systems using chemical solvents, such as MEA or chilled ammonia scrubbing. Retrofits of these systems to the same reference coal-fired power plant resulted in net efficiency penalties of 9.5 and 9%$_{HHV}$ points, and energy penalties of 24.7 and 23.3%$_{HHV}$, respectively [29,67]. The specific coal consumption increased in these retrofit scenarios by 32.8 and 30.3%, respectively. Therefore, the HCP-MAAM retrofit scenario has the potential to reduce the impact of the CO_2 capture system on the performance of coal-fired power plants.

The analysis of the energy requirement of the CO_2 capture system using HCP-MAAM sorbent revealed that the specific heat requirement of the HCP-MAAM sorbent (2.1–2.2 $MJ_{th}/kgCO_2$) was as good as or superior to the specific heat requirement reported for the following solvents: Cansolv (2.33 $MJ_{th}/kgCO_2$), K_2CO_3 (2–2.5 $MJ_{th}/kgCO_2$), Econamine FG + (3.12 $MJ_{th}/kgCO_2$), and MDEA-PZ (2.52 $MJ_{th}/kgCO_2$)

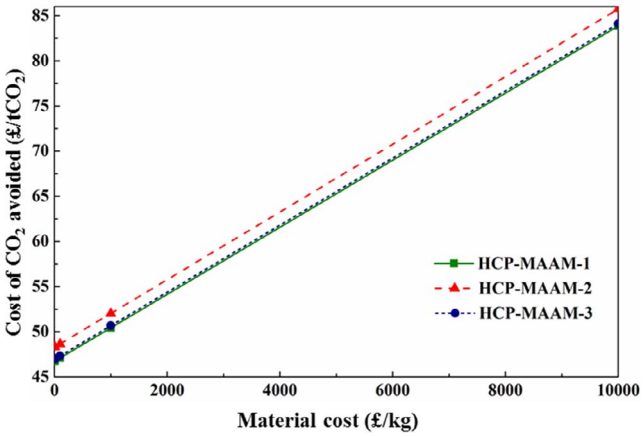

Fig. 10. Effect of the material cost on the cost of CO_2 avoided.

[68]. As a result, the steam extraction accounted only for 29.3–29.6% of the parasitic load in the HCP-MAAM retrofit, as opposed to about 60% in the chemical solvent scrubbing retrofit scenarios [67].

The economic assessment (Table 4) revealed that retrofitting an HCP-MAAM-based CO_2 capture system will result in an increase of the specific capital cost of the entire system by 72.6–75.0% (843.6–870.9 £/$kW_{el,gross}$) compared to the specific capital cost of the reference coal-fired power plant (1161.3 £/$kW_{el,gross}$). Importantly, the key economic indicators for the HCP-MAAM retrofit scenarios fall within the ranges reported previously for coal-fired power plants retrofitted with CO_2 capture systems using chemical solvents (AC = 30–60 £/tCO_2 [69–72]). Furthermore, the sensitivity analysis (Fig. 10) performed on the material cost indicated that the economic performance of the HCP-MAAM-based CO_2 capture system will remain comparable to the chemical solvent scrubbing system even if the material cost is as high as 3000–3500 £/kg. However, this is based on the assumption that no material degradation occurs over multiple cycles; if this were untrue, the cost of the material would be an important component of the operating cost of the system. Considering lower impact on the thermodynamic performance of the reference coal-fired power plant, the HCP-MAAM retrofit scenario can be expected to bring higher profit from electricity sales compared to the chemical solvent scrubbing retrofit scenarios.

4. Conclusions

Nitrogen-rich hyper-crosslinked polymeric materials (HCP-MAAM) were synthesised by copolymerisation of MAAM and EGDMA through bulk polymerisation. The presence of polar amide groups within the polymer network resulted in a high affinity of the material towards CO_2

Table 4
A summary of techno-economic performance indicators.

Parameter	Reference coal-fired power plant	HCP-MAAM-1 retrofit scenario	HCP-MAAM-2 retrofit scenario	HCP-MAAM-3 retrofit scenario
Thermodynamic performance indicators				
Gross power output (MW_{el})	580.4	539.7	540.1	538.8
Net power output (MW_{el})	552.7	441.9	438.6	441.7
Net thermal efficiency (%$_{HHV}$)	38.5	30.8	30.5	30.8
Specific coal consumption ($g/kW_{el}h$)	350.3	438.0	441.4	438.2
Specific CO_2 emission ($g/kW_{el}h$)	792.3	99.0	99.8	99.0
Net efficiency penalty (%$_{HHV}$ points)	–	7.7	8.0	7.7
Increase in specific coal consumption (%)	–	25.1	26.0	25.1
Specific heat requirement ($MJ_{th}/kgCO_2$)	–	2.1	2.2	2.2
Economic performance indicators				
Specific capital cost (£/$kW_{el,gross}$)	1161.3	2004.9	2032.2	2011.9
Levelised cost of electricity (£/$MW_{el}h$)	36.9	69.1	70.5	69.7
CO_2 avoided cost (£/tCO_2)	–	46.2	48.3	47.0

at low pressures, while the associated heat of adsorption was relatively low, 28–35 kJ/mol. A maximum CO_2/N_2 selectivity (at a CO_2:N_2 ratio of 15:85) of 52 (corresponding to 91% purity of the gas stream after regeneration) was achieved for HCP-MAAM-3 polymer. An increase in the density of amide groups within the polymer network led to a higher affinity towards CO_2, but resulted in a higher heat of adsorption and a reduction in CO_2 adsorption capacity. The highest CO_2 adsorption capacity was 1.56 mmol/g, measured at 273 K.

The techno-economic analysis showed that retrofitting a HCP-MAAM-based CO_2 capture system to a 580-MW coal-fired power plant resulted in a net efficiency penalty of 7.7–8.0%$_{HHV}$ points, which was lower than those for MEA and chilled ammonia scrubbing retrofit scenarios. Moreover, the economic performance of the HCP-MAAM-based CO_2 capture system was found to be comparable to that for chemical solvent scrubbing, even up to a material cost of 3500 £/kg.

Accordingly, a combination of low energy required for regeneration, high selectivity, high density, high thermal resistance, and chemical inertness can potentially make HCP-MAAM polymers a promising candidate for post-combustion carbon capture.

Notes

The authors declare no competing financial interest.

Acknowledgement

The authors gratefully acknowledge the financial support for this work by coERCe granted by Innovate UK, project Grant: 102213, and Cambridge Engineering and Analysis Design (CEAD) Ltd. The authors would like to thank Monika Pietrzak, Rob Bentham, and Kim Robertshaw for their help and support during the entire experimental work.

Appendix A. Supplementary data

Supplementary data associated with this article can be found, in the online version, at http://dx.doi.org/10.1016/j.cej.2017.11.106.

References

[1] CCC, Reducing emissions and preparing for climate change: 2015 progress report to parliament summary and recommendations, United Kingdom, 2015. www.theccc.org.uk.
[2] DECC, CCS Roadmap. Supporting deployment of carbon capture and storage in the UK, 2012. doi: URN 12D/016.
[3] M.D. Aminu, S.A. Nabavi, C.A. Rochelle, V. Manović, A review of developments in carbon dioxide storage, Appl. Energy (2017), http://dx.doi.org/10.1016/j.apenergy.2017.09.015.
[4] D.M. D'Alessandro, B. Smit, J.R. Long, Carbon dioxide capture: prospects for new materials, Angew. Chem. Int. Ed. 49 (2010) 6058–6082, http://dx.doi.org/10.1002/anie.201000431.
[5] J. Wang, L. Huang, R. Yang, Z. Zhang, J. Wu, Y. Gao, Q. Wang, D. O'Hare, Z. Zhong, Recent advances in solid sorbents for CO_2 capture and new development trends, Energy Environ. Sci. 7 (2014) 3478–3518, http://dx.doi.org/10.1039/C4EE01647E.
[6] E.F. da Silva, A.M. Booth, Emissions from postcombustion CO_2 capture plants, Environ. Sci. Technol. 47 (2013) 659–660, http://dx.doi.org/10.1021/es305111u.
[7] T.C. Drage, C.E. Snape, L.A. Stevens, J. Wood, J. Wang, A.I. Cooper, R. Dawson, X. Guo, C. Satterley, R. Irons, Materials challenges for the development of solid sorbents for post-combustion carbon capture, J. Mater. Chem. 22 (2012) 2815–2823, http://dx.doi.org/10.1039/C2JM12592G.
[8] F.Q. Liu, L. Wang, Z.G. Huang, C.Q. Li, W. Li, R.X. Li, W.H. Li, Amine-tethered adsorbents based on three-dimensional macroporous silica for CO_2 capture from simulated flue gas and air, ACS Appl. Mater. Interfaces 6 (2014) 4371–4381, http://dx.doi.org/10.1021/am500089g.
[9] A.S. Jalilov, G. Ruan, C.C. Hwang, D.E. Schipper, J.J. Tour, Y. Li, H. Fei, E.L.G. Samuel, J.M. Tour, Asphalt-derived high surface area activated porous carbons for carbon dioxide capture, ACS Appl. Mater. Interfaces 7 (2015) 1376–1382, http://dx.doi.org/10.1021/am508858x.
[10] D.S. Zhang, Z. Chang, Y.F. Li, Z.Y. Jiang, Z.H. Xuan, Y.H. Zhang, J.R. Li, Q. Chen, T.L. Hu, X.H. Bu, Fluorous metal-organic frameworks with enhanced stability and high H_2/CO_2 storage capacities, Sci. Rep. 3 (2013) 3312–3318, http://dx.doi.org/10.1038/srep03312.
[11] Z. Chang, D.S. Zhang, Q. Chen, X.H. Bu, Microporous organic polymers for gas storage and separation applications, Phys, Chem. Chem. Phys. 15 (2013) 5430–5442, http://dx.doi.org/10.1039/C3CP50517K.
[12] M.E. Boot-Handford, J.C. Abanades, E.J. Anthony, M.J. Blunt, S. Brandani, N. Mac Dowell, J.R. Fernández, M.C. Ferrari, R. Gross, J.P. Hallett, R.S. Haszeldine, P. Heptonstall, A. Lyngfelt, Z. Makuch, E. Mangano, R.T.J. Porter, M. Pourkashanian, G.T. Rochelle, N. Shah, J.G. Yao, P.S. Fennell, Carbon capture and storage update, Energy Environ. Sci. 7 (2014) 130–189, http://dx.doi.org/10.1039/c3ee42350f.
[13] S.A. Nabavi, G.T. Vladisavljevic, A. Wicaksono, S. Georgiadou, V. Manovic, Production of molecularly imprinted polymer particles with amide-decorated cavities for CO_2 capture using membrane emulsification/suspension polymerisation, Colloids Surf., A 521 (2017) 231–238, http://dx.doi.org/10.1016/j.colsurfa.2016.05.033.
[14] S.A. Nabavi, G.T. Vladisavljević, E.M. Eguagie, B. Li, S. Georgiadou, V. Manović, Production of spherical mesoporous molecularly imprinted polymer particles containing tunable amine decorated nanocavities with CO_2 molecule recognition properties, Chem. Eng. J. 306 (2016) 214–225, http://dx.doi.org/10.1016/j.cej.2016.07.054.
[15] H.A. Patel, S.H. Je, J. Park, D.P. Chen, Y. Jung, C.T. Yavuz, A. Coskun, Unprecedented high-temperature CO_2 selectivity in N_2-phobic nanoporous covalent organic polymers, Nat. Commun. 4 (2013) 1357–1364, http://dx.doi.org/10.1038/ncomms2359.
[16] Z. Xiang, X. Zhou, C. Zhou, S. Zhong, X. He, C. Qin, D. Cao, Covalent-organic polymers for carbon dioxide capture, J. Mater. Chem. 22 (2012) 22663–22669, http://dx.doi.org/10.1039/c2jm35446b.
[17] R.T.J. Porter, M. Fairweather, M. Pourkashanian, R.M. Woolley, The range and level of impurities in CO_2 streams from different carbon capture sources, Int. J. Greenhouse Gas Control 36 (2015) 161–174, http://dx.doi.org/10.1016/j.ijggc.2015.02.016.
[18] J.R. Li, R.J. Kuppler, H.C. Zhou, Selective gas adsorption and separation in metal-organic frameworks, Chem. Soc. Rev. 38 (2009) 1477–1504, http://dx.doi.org/10.1039/B802426J.
[19] K. Sumida, D.L. Rogow, J.A. Mason, T.M. McDonald, E.D. Bloch, Z.R. Herm, T.H. Bae, J.R. Long, Carbon dioxide capture in metal-organic frameworks, Chem. Rev. 112 (2012) 724–781, http://dx.doi.org/10.1021/cr2003272.
[20] Z. Chen, S. Deng, H. Wei, B. Wang, J. Huang, G. Yu, Polyethylenimine-impregnated resin for high CO_2 adsorption: an efficient adsorbent for CO_2 capture from simulated flue gas and ambient air, ACS Appl. Mater. Interfaces 5 (2013) 6937–6945, http://dx.doi.org/10.1021/am400661b.
[21] W. Choi, K. Min, C. Kim, Y.S. Ko, J.W. Jeon, H. Seo, Y.K. Park, M. Choi, Epoxide-functionalization of polyethyleneimine for synthesis of stable carbon dioxide adsorbent in temperature swing adsorption, Nat. Commun. 7 (2016) 12640–12648, http://dx.doi.org/10.1038/ncomms12640.
[22] T. Remy, S.A. Peter, S. Van der Perre, P. Valvekens, D.E. De Vos, G.V. Baron, J.F.M. Denayer, Selective dynamic CO_2 separations on Mg-MOF-74 at low pressures: a detailed comparison with 13X, J. Phys. Chem. C. 117 (2013) 9301–9310, http://dx.doi.org/10.1021/jp401923v.
[23] J. Liu, N. Sun, C. Sun, H. Liu, C. Snape, K. Li, W. Wei, Y. Sun, Spherical potassium intercalated activated carbon beads for pulverised fuel CO_2 post-combustion capture, Carbon 94 (2015) 243–255, http://dx.doi.org/10.1016/j.carbon.2015.06.036.
[24] Y. Zhao, Y. Shen, L. Bai, R. Hao, L. Dong, Synthesis and CO_2 adsorption properties of molecularly imprinted adsorbents, Environ. Sci. Technol. 46 (2012) 1789–1795, http://dx.doi.org/10.1021/es203580b.
[25] S.A. Nabavi, G.T. Vladisavljević, Y. Zhu, V. Manović, Synthesis of size-tunable CO_2-philic imprinted polymeric particles (MIPs) for low-pressure CO_2 capture using oil-in-oil suspension polymerization, Environ. Sci. Technol. 51 (2017) 11476–11483, http://dx.doi.org/10.1021/acs.est.7b03259.
[26] R.A. Lorenzo, A.M. Carro, C. Alvarez-Lorenzo, A. Concheiro, To remove or not to remove? The challenge of extracting the template to make the cavities available in molecularly imprinted polymers (MIPs), Int. J. Mol. Sci. 12 (2011) 4327–4347, http://dx.doi.org/10.3390/ijms12074327.
[27] B. Erdem, R.A. Hunsicker, G.W. Simmons, E.D. Sudol, V.L. Dimonie, M.S. El-aasser, XPS and FTIR surface characterization of TiO_2 particles used in polymer encapsulation, Langmuir 17 (2001) 2664–2669, http://dx.doi.org/10.1021/la0015213.
[28] D.P. Hanak, C. Biliyok, V. Manović, Rate-based model development, validation and analysis of chilled ammonia process as an alternative CO_2 capture technology for coal-fired power plants, Int. J. Greenhouse Gas Control 34 (2015) 52–62, http://dx.doi.org/10.1016/j.ijggc.2014.12.013.
[29] D.P. Hanak, C. Biliyok, V. Manović, Efficiency improvements for the coal-fired power plant retrofit with CO_2 capture plant using chilled ammonia process, Appl. Energy 151 (2015) 258–272, http://dx.doi.org/10.1016/j.apenergy.2015.04.059.
[30] J. Black, Cost and performance baseline for fossil energy plants volume 1: Bituminous coal and natural gas to electricity, 2013.
[31] D.P. Hanak, C. Biliyok, V. Manović, Evaluation and modeling of part-load performance of coal-fired power plant with postcombustion CO_2 capture, Energy Fuels 29 (2015) 3833–3844, http://dx.doi.org/10.1021/acs.energyfuels.5b00591.
[32] H.H. Rachford Jr., J.D. Rice, Procedure for use of electronic digital computers in calculating flash vaporization hydrocarbon equilibrium, J. Pet. Technol. 4 (1952) 327–328, http://dx.doi.org/10.2118/952327-G.
[33] L.M. Romeo, J.C. Abanades, J.M. Escosa, J. Paño, A. Giménez, A. Sánchez-Biezma, J.C. Ballesteros, Oxyfuel carbonation/calcination cycle for low cost CO_2 capture in existing power plants, Energy Convers. Manag. 49 (2008) 2809–2814, http://dx.doi.org/10.1016/j.enconman.2008.03.022.
[34] D.P. Hanak, E.J. Anthony, V. Manović, A review of developments in pilot-plant

testing and modelling of calcium looping process for CO_2 capture from power generation systems, Energy Environ. Sci. 8 (2015) 2199–2249, http://dx.doi.org/10.1039/C5EE01228G.
[35] I. Pfaff, J. Oexmann, A. Kather, Optimised integration of post-combustion CO_2 capture process in greenfield power plants, Energy 35 (2010) 4030–4041, http://dx.doi.org/10.1016/j.energy.2010.06.004.
[36] S. Posch, M. Haider, Optimization of CO_2 compression and purification units (CO_2CPU) for CCS power plants, Fuel 101 (2012) 254–263, http://dx.doi.org/10.1016/j.fuel.2011.07.039.
[37] T. Sanpasertparnich, R. Idem, I. Bolea, D. deMontigny, P. Tontiwachwuthikul, Integration of post-combustion capture and storage into a pulverized coal-fired power plant, Int. J. Greenhouse Gas Control 4 (2010) 499–510, http://dx.doi.org/10.1016/j.ijggc.2009.12.005.
[38] B. Metz, O. Davidson, H. de Coninck, M. Loos, L. Meyer, IPCC special report on carbon dioxide capture and storage, Cambridge, United Kingdom and New York, NY, USA, 2005.
[39] Y. Yang, R. Zhai, L. Duan, M. Kavosh, K. Patchigolla, J. Oakey, Integration and evaluation of a power plant with a CaO-based CO_2 capture system, Int. J. Greenhouse Gas Control 4 (2010) 603–612, http://dx.doi.org/10.1016/j.ijggc.2010.01.004.
[40] J.C. Abanades, G. Grasa, M. Alonso, N. Rodriguez, E.J. Anthony, L.M. Romeo, Cost structure of a postcombustion CO_2 capture system using CaO, Environ. Sci. Technol. 41 (2007) 5523–5527, http://dx.doi.org/10.1021/es070099a.
[41] M. Zhao, A.I. Minett, A.T. Harris, A review of techno-economic models for the retrofitting of conventional pulverised-coal power plants for post-combustion capture (PCC) of CO_2, Energy Environ. Sci. 6 (2013) 25–40, http://dx.doi.org/10.1039/C2EE22890D.
[42] R.H. Perry, D.W. Green, J.O. Aloney, Perry's Chemical Engineers' Handbook, McGraw-Hill, New York, 2007.
[43] NETL, Technology readiness assessment – overview. Pathway for readying the next generation of affordable clean energy technology – Carbon Capture, Utilization, and Storage (CCUS) FutureGen Alliance, Pittsburgh, PA, USA, 2012.
[44] R.D. Woods, Rules of Thumb in Engineering Practice, Wiley-VCH Verlag GmbH & Co. KGaA, Weinheim, Germany, 2007.
[45] K.S.W. Sing, D.H. Everett, R.A.W. Haul, L. Moscou, R.A. Pierotti, J. Rouquérol, T. Siemieniewska, Reporting physisorption data for gas/solid systems with special reference to the determination of surface area and porosity, Pure Appl. Chem. 57 (1985) 603–619, http://dx.doi.org/10.1351/pac198557040603.
[46] C. Weidenthaler, Pitfalls in the characterization of nanoporous and nanosized materials, Nanoscale 3 (2011) 792–810, http://dx.doi.org/10.1039/C0NR00561D.
[47] T.M. McDonald, W.R. Lee, J.A. Mason, B.M. Wiers, C.S. Hong, J.R. Long, Capture of carbon dioxide from air and flue gas in the alkylamine-appended metal-organic framework mmen-Mg_2(dobpdc), J. Am. Chem. Soc. 134 (2012) 7056–7065, http://dx.doi.org/10.1021/ja300034j.
[48] A.L. Myers, J.M. Prausnitz, Thermodynamics of mixed-gas adsorption, AIChE J. 11 (1965) 121–127, http://dx.doi.org/10.1002/aic.690110125.
[49] L.M. Azofra, M. Altarsha, M.F. Ruiz-López, F. Ingrosso, A theoretical investigation of the CO_2-philicity of amides and carbamides, Theor. Chem. Acc. 132 (2013) 1326–1334, http://dx.doi.org/10.1007/s00214-012-1326-4.
[50] W.C. Song, X.K. Xu, Q. Chen, Z.Z. Zhuang, X.H. Bu, Nitrogen-rich diaminotriazine-based porous organic polymers for small gas storage and selective uptake, Polym. Chem. 4 (2013) 4690–4696, http://dx.doi.org/10.1039/C3PY00590A.
[51] M. Perera, R. Gamage, T. Rathnaweera, A. Ranathunga, A. Koay, X. Choi, A review of CO_2-enhanced oil recovery with a simulated sensitivity analysis, Energies 9 (2016) 481–502, http://dx.doi.org/10.3390/en9070481.
[52] M. Kaliva, G.S. Armatas, M. Vamvakaki, Microporous polystyrene particles for selective carbon dioxide capture, Langmuir 28 (2012) 2690–2695, http://dx.doi.org/10.1021/la204991n.
[53] Y. Zhao, H. Ding, Q. Zhong, Synthesis and characterization of MOF-aminated graphite oxide composites for CO_2 capture, Appl. Surf. Sci. 284 (2013) 138–144, http://dx.doi.org/10.1016/j.apsusc.2013.07.068.
[54] S. Zulfiqar, S. Awan, F. Karadas, M. Atilhan, C.T. Yavuz, M.I. Sarwar, Amidoxime porous polymers for CO_2 capture, RSC Adv. 3 (2013) 17203–17213, http://dx.doi.org/10.1039/C3RA42433B.
[55] M. Saleh, S. Bin Baek, H.M. Lee, K.S. Kim, Triazine-based microporous polymers for selective adsorption of CO_2, J. Phys. Chem. C 119 (2015) 5395–5402, http://dx.doi.org/10.1021/jp509188h.
[56] R. Dawson, D.J. Adams, A.I. Cooper, Chemical tuning of CO_2 sorption in robust nanoporous organic polymers, Chem. Sci. 2 (2011) 1173–1177, http://dx.doi.org/10.1039/c1sc00100k.
[57] Y.Q. Chen, Y.K. Qu, G.R. Li, Z.Z. Zhuang, Z. Chang, T.L. Hu, J. Xu, X.H. Bu, Zn(II)-benzotriazolate clusters based amide functionalized porous coordination polymers with high CO_2 adsorption selectivity, Inorg. Chem. 53 (2014) 8842–8844, http://dx.doi.org/10.1021/ic500788z.
[58] J.A. Mason, K. Sumida, Z.R. Herm, R. Krishna, J.R. Long, Evaluating metal-organic frameworks for post-combustion carbon dioxide capture via temperature swing adsorption, Energy Environ. Sci. 4 (2011) 3030–3040, http://dx.doi.org/10.1039/C1EE01720A.
[59] H. Furukawa, O.M. Yaghi, Storage of hydrogen, methane, and carbon dioxide in highly porous covalent organic frameworks for clean energy applications, J. Am. Chem. Soc. 131 (2009) 8875–8883, http://dx.doi.org/10.1021/ja9015765.
[60] W. Lu, J.P. Sculley, D. Yuan, R. Krishna, Z. Wei, H.C. Zhou, Polyamine-tethered porous polymer networks for carbon dioxide capture from flue gas, Angew. Chem. Int. Ed. 51 (2012) 7480–7484, http://dx.doi.org/10.1002/anie.201202176.
[61] Q. Gao, J. Xu, D. Cao, Z. Chang, X.H. Bu, A rigid nested metal–organic framework featuring a thermoresponsive gating effect dominated by counterions, Angew. Chem. 128 (2016) 15251–15254, http://dx.doi.org/10.1002/ange.201608250.
[62] W. Lu, D. Yuan, J. Sculley, D. Zhao, R. Krishna, H.-C. Zhou, Sulfonate-grafted porous polymer networks for preferential CO_2 adsorption at low pressure, J. Am. Chem. Soc. 133 (2011) 18126–18129, http://dx.doi.org/10.1021/ja2087773.
[63] R.V. Siriwardane, M.S. Shen, E.P. Fisher, J.A. Poston, Adsorption of CO_2 on molecular sieves and activated carbon, Energy Fuels 15 (2001) 279–284, http://dx.doi.org/10.1021/ef000241s.
[64] S. Sung, M.P. Suh, Highly efficient carbon dioxide capture with a porous organic polymer impregnated with polyethylenimine, J. Mater. Chem. A 2 (2014) 13245–13249, http://dx.doi.org/10.1039/C4TA02861A.
[65] H. Kim, H.J. Cho, S. Narayanan, S. Yang, H. Furukawa, S. Schiffres, X. Li, Y.-B. Zhang, J. Jiang, O.M. Yaghi, E.N. Wang, Characterization of adsorption enthalpy of novel water-stable zeolites and metal-organic frameworks, Sci. Rep. 6 (2016) 19097–19104, http://dx.doi.org/10.1038/srep19097.
[66] Y.E. Kim, S.J. Moon, Y. Il Yoon, S.K. Jeong, K.T. Park, S.T. Bae, S.C. Nam, Heat of absorption and absorption capacity of CO_2 in aqueous solutions of amine containing multiple amino groups, Sep. Purif. Technol. 122 (2014) 112–118, http://dx.doi.org/10.1016/j.seppur.2013.10.030.
[67] D.P. Hanak, C. Biliyok, E.J. Anthony, V. Manović, Modelling and comparison of calcium looping and chemical solvent scrubbing retrofits for CO_2 capture from coal-fired power plant, Int. J. Greenhouse Gas Control 42 (2015) 226–236, http://dx.doi.org/10.1016/j.ijggc.2015.08.003.
[68] K. Goto, K. Yogo, T. Higashii, A review of efficiency penalty in a coal-fired power plant with post-combustion CO_2 capture, Appl. Energy 111 (2013) 710–720, http://dx.doi.org/10.1016/j.apenergy.2013.05.020.
[69] ZEP, The costs of CO2 capture, transport and storage, 2011.
[70] P. Versteeg, E.S. Rubin, A technical and economic assessment of ammonia-based post-combustion CO_2 capture at coal-fired power plants, Int. J. Greenhouse Gas Control 5 (2011) 1596–1605, http://dx.doi.org/10.1016/j.ijggc.2011.09.006.
[71] N.M. Dowell, N. Shah, The multi-period optimisation of an amine-based CO_2 capture process integrated with a super-critical coal-fired power station for flexible operation, Comput. Chem. Eng. 74 (2015) 169–183, http://dx.doi.org/10.1016/j.compchemeng.2015.01.006.
[72] E.S. Rubin, J.E. Davison, H.J. Herzog, The cost of CO_2 capture and storage, Int. J. Greenhouse Gas Control 40 (2015) 378–400, http://dx.doi.org/10.1016/j.ijggc.2015.05.018.